Available online at www.sciencedirect.com
SCIENCE DIRECT®
International Journal of Heat and Mass Transfer 48 (2005) 2473–2482
International Journal of HEAT and MASS TRANSFER
www.elsevier.com/locate/ijhmt

Experimental study of heat transfer in oscillating flow

Pascale Bouvier *, Pascal Stouffs [1], Jean-Pierre Bardon

Laboratoire de Thermocinétique, UMR CNRS 6607, Ecole Polytechnique de l'Université de Nantes, BP 50609, 44306 Nantes, France

Received 25 September 2003; received in revised form 8 November 2004
Available online 7 April 2005

Abstract

This paper describes an experimental study of heat transfer in oscillating flow inside a cylindrical tube. Profiles of temperature are taken inside the wall and in the fluid from an instrumented test rig, in different conditions of oscillating flow. Profiles obtained allow the observation of the wall effect on heat transfer. A method using the inverse heat conduction principle allows the characterization of local heat transfers at the fluid–solid interface. Finally, a comparison between global and local approaches of heat transfer shows the difficulty of defining a dimensionless heat flux density to model local heat transfer in oscillating flow.

1. Introduction

Understanding the processes of heat and mass transport in oscillatory flow is a topic of interest for many applications ranging from tidal estuaries [1] and novel heat exchangers [2] to the field of pulmonary physiology [3]. Notably, flow through heat exchangers tubes of Stirling engines is oscillatory. In these engines, the temperature of the working fluid is submitted to hard periodic variations essentially due to cyclic variations of the pressure [4]. To more adequately predict the engine performance, it is necessary to have models of local heat transfer between oscillatory flow and the wall of heat exchanger. Indeed, the flow frequency is such that a quasi-stationary approach is not acceptable [5]. So, several studies have been initiated to better understand the nature of oscillatory flows and the effect of the flow oscillation on fluid mechanics and heat transfer in Stirling engines heat exchangers [5,6].

Concerning fluid mechanics, there is a lot of studies about transition from laminar flow to turbulence which allowed the elaboration of the well known Glimp's Diagram [6,7]. However, concerning heat transfer, studies are more sparce and most of them consider the wall temperature of heat exchangers as a constant [8–10].

In this paper, we report results of an experimental investigation, carried out in the Laboratoire de Thermocinétique, dealing with heat transfer in oscillating flow with a time mean velocity of zero. The pipe geometry is circular. The test rig used has been designed to produce oscillating flow conditions found in most Stirling engines in term of characteristics parameters such as the Reynolds number based on the amplitude of the bulk mean velocity Re_{max}, the dimensionless frequency

* Corresponding author. Present address: Laboratoire d' Energétique, HEI, 13 rue de Toul, 59046 Lille, France. Tel.: +33 3 28 38 48 58; fax: +33 3 28 38 48 04.
E-mail address: pascale.bouvier@hei.fr (P. Bouvier).
[1] Present address: Laboratoire de Thermique, Energétique et Procédés (LaTEP, EA 1932),Université de Pau, IUT—GTE, Avenue de l'Université, 64000 Pau, France.

0017-9310/$ - see front matter © 2005 Elsevier Ltd. All rights reserved.
doi:10.1016/j.ijheatmasstransfer.2005.01.037

Nomenclature

A_r	$=2x_{m,\max}/L_t$ amplitude of fluid displacement
D_t	internal diameter of the tube, m
e_W	wall thickness of the tube, m
f	frequency, Hz
k	heat conductivity, W/m K
L_t	tube length, m
Nu	Nusselt number
$Re_{\max}$	$=u_{m,\max}D_t/\nu$, Reynolds number based on the amplitude of the bulk mean velocity
Re_ω	$=\omega D_t^2/4\nu$ dimensionless frequency
R_t	tube radius, m
r	radial coordinate in fluid from the fluid/solid interface, m
t	times, s
T	temperature, K
T_b	bulk temperature, K
T_w	wall temperature, K
$u(T)$	uncertainty on temperature T
$u_{m,\max}$	amplitude of bulk mean velocity, m/s
x	radial location in tube wall, m
x_1	=206.3 μm in tube wall from the interface solid/fluid
x_2	=405.2 μm in tube wall from the interface solid/fluid
x_3	=624.6 μm in tube wall from the interface solid/fluid
Y	Fourier transform

Greek symbols

δ_s	experimental skin thickness, m
$\delta_{s,theo}$	theoretical skin thickness, m
ϕ	heat flux density, W/m^2
ϕ_{ref}	heat flux density used as reference, W/m^2
ϕ^*	$=\phi/\phi_{ref}$, dimensionless heat flux density
κ	heat diffusivity, m^2/s
ν	kinematic viscosity, m^2/s
ω	angular velocity, rad/s
ψ	phase shift, rad

Subscripts

ext	referred to external wall of the tube
f	referred to fluid
s	referred to solid
p	permanent
u	unsteady
0	at the fluid–solid interface
$\overline{A}$	temporal mean of the quantity A
1	referred to location x_1
2	referred to location x_2
3	referred to location x_3

Re_ω and the amplitude of fluid displacement A_r. The pipe wall is heated and flow entries are cooled.

We describe what we call "a parietal captor", which is in fact a micro-instrumentation in the thickness of the tube wall which allows to determine surface heat flux and wall temperature. We also present a mobile probe in the fluid, used to measure instantaneous temperature profiles at mid-length of the test section at several radial positions.

These measurements should allow us to better understand heat transfer in oscillatory flows and to verify the hypothesis which consists of considering the wall temperature as a constant. Results should show if temporal variations of wall temperature are effectively negligible with respect to those found in the fluid. Nevertheless, they should allow us to characterize local heat transfer at the fluid–solid interface and to observe the effect of the wall on heat transfer.

In the first part, we describe the test rig and its associated instrumentation. In the second part, we present temperatures profiles in the wall. In the third part, we propose a method of characterization of local heat transfer. Finally, we open a discussion about the dimensionless heat flux density in oscillatory flow.

2. Experimental apparatus

2.1. Description of the test rig

The test section is a circular tube made of stainless steel, 5.7 m long, of 48.3 mm ext. dia., with a thickness of 3.2 mm. At its extremities, the tube is connected to a convergent linked to an heat exchanger. Air is cooled by water maintained at a controlled temperature. The flow delivery section is connected to the heat exchangers with flexible tubes.

The drive assembly generates oscillating flow of air with a time averaged velocity of zero in the test section. It is made of two coupled scotch-yokes linked to a flywheel of 600 mm dia., with a mass of 80 kg, on which we can adjust five different strokes. Each scotch-yoke drives two pistons of 260 mm dia. The flywheel is driven by a motoreductor of 49 rpm linked with pulleys. The pulleys agency allows us to vary the dimensionless frequency Re_ω. Finally, with this mechanical device, we can obtain the working domain of the rig in terms of $Re_{\max}$ and Re_ω, represented in Fig. 1, by connecting one, two, three or four pistons to the test section.

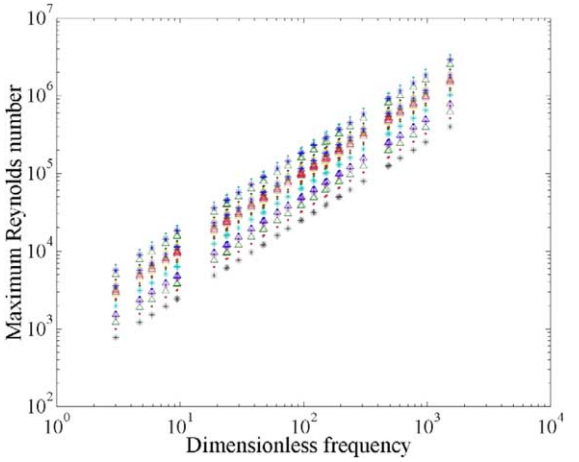

Fig. 1. Working domain of the test rig.

In this paper, we present results of measurements taken at mid-length of the test section, where the flow is hydrodynamically developed [5]. For the thermal measures, there is an electric band heater of 76 cm long wrapped around the tube, at mid-length of the test section [11]. Heat is evacuated by heat exchangers at the extremities of the test section (see Fig. 2).

2.2. Thermal instrumentation

A mobile probe, built at the laboratory, is provided with a thermocouple of 12 μm, tightened between two thin tubes, taken sufficiently far away from each other in order to avoid edges effects [12]. We sealed two thin metallic needles on the tubes to detect wall by electric contact. The characteristics of the sensor has been studied in [11]. In the domain of $1000 < Re_{max} < 2 \times 10^4$, its response time is less than 2×10^{-2} s. For higher values of Re_{max}, it is less than 5×10^{-3} s. This probe can approach the wall up to 185 μm with an uncertainty of 3 μm. Radial profiles of instantaneous fluid temperature are taken by moving the probe along the tube radius by means of a micrometric screw (0–50 mm ± 0.005 mm).

Moreover a micro-thermal instrumentation inside one element of the tube was realized by the laboratory. This element with its instrumentation is called "parietal sensor" because it allows us to determine instantaneous flux and temperature at the fluid–solid interface. This element is cut up in the tube and worked in order to insert 3 micro-thermocouples at different radial positions, then replaced and sealed on the tube. All the cuts are made in planes parallel to the heat flux direction, so that the thermal field is not disturbed. Chromel and alumel wires of 25 μm diameter which constitute these micro-thermocouples are disposed and sealed in the axial direction of the tube perpendicularly to the direction of heat flux. Their micro-junctions are soldered in the thickness of the tube wall, perpendicularly to the radius, near the fluid–solid interface. The nearest position, x_1 is at 206.3 μm from the fluid–solid interface, the second position, x_2 at 405.2 μm and the third position, x_3 at 624.6 μm. A farther thermocouple of 80 μm diameter is soldered on the external face of the tube. By using inverse heat conduction methods [13], this "parietal sensor" allows us to determine instantaneous heat flux density and temperature at the solid–fluid interface.

Due to the noise level, the uncertainty on all temperature measurements is estimated to $u(T) = 0.075$ °C [11].

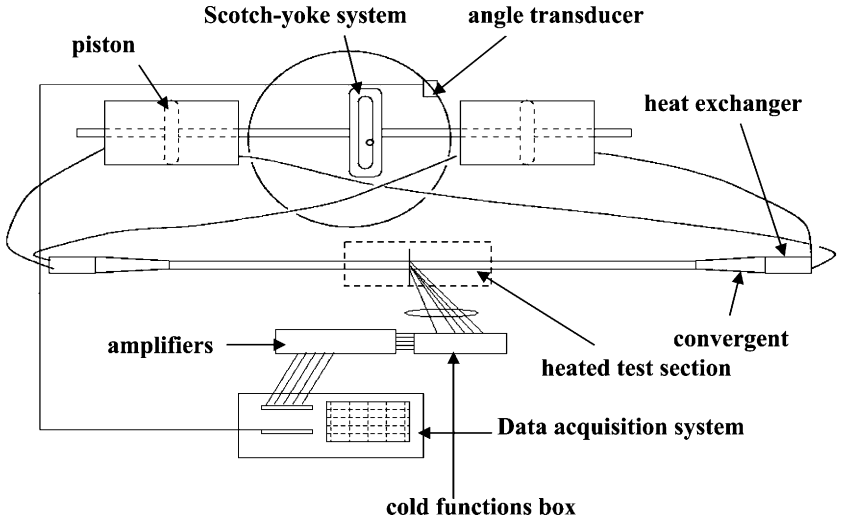

Fig. 2. Test rig assembly.

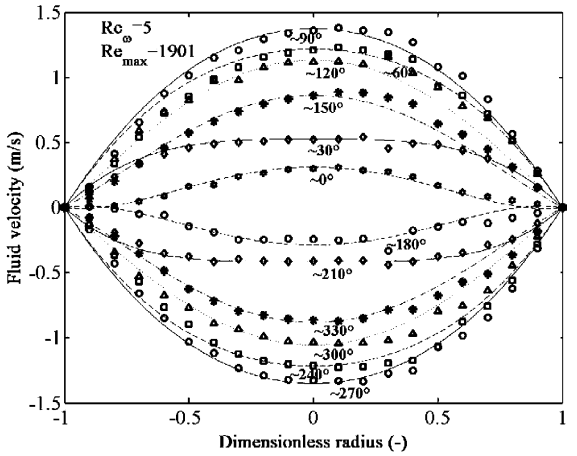

Fig. 3. Superposition of analytical profiles (lines) and experimental profiles (symbols) of velocity every 30° of phase angle.

2.3. Validation of the test rig

In order to verify the validity of the drive assembly, we measured radial velocity profiles, at mid-length of the test section, by replacing the middle part of the tube by a Plexiglas tube of the same length. The test section has been seeded by smog and measures are taken every 30° crank angle with the aid of a photoelectric detector, in hydrodynamically developed flow conditions [11]. In Fig. 3, we superimpose the analytical solution, obtained by the resolution of the conservative equation of movement [14–16] in laminar oscillatory flow. We verify that the flow is purely sinusoidal and axisymmetric [11,17].

In conditions of transition of oscillating flow, we observed a laminar flow during flow accelerations and a turbulent flow during flow decelerations, in the same oscillation cycle. From our experimental measures, we cannot propose a theoretical model that would take into account the intermittent appearance of the turbulence. It is a difficult problem that we cannot address at present. The transition is studied with more details in [18] where no accurate transition criterion is proposed.

3. Influence of the metallic wall on heat transfer

3.1. Validation of the measures in the wall

In this second part of our work, we imposed a constant heat flux density, ϕ_{ext}, at the external wall of the tube whereas the flow is periodic in the tube.

For cases characterized by small Reynolds number Re_{max} and dimensionless frequency Re_ω, amplitudes of temperature variations were too small to be detected [8]. For other cases, like ($Re_{max} = 160163$, $Re_\omega = 144.15$), measures translated real physics phenomena since they allow us to find values of the skin thickness δ_s in good agreement with the theoretical values $\delta_{s,theo} = \sqrt{\frac{2\kappa_s}{\omega}}$. In the cases where $e_W \gg \delta_{s,theo}$ and $e_W \ll R_t$, considering that the wall excitation frequency corresponds to twice the frequency of the piston motion, the wall is submitted to an excitation like

$$T = T_0 \cos(\omega t) \tag{1}$$

with $\omega = 2\pi(2f_p)$ where f_p is the frequency of the piston motion. The temperature signal can be written as follows:

$$T(x_i, t) = A_0 e^{\frac{-x_i}{\delta_s}} \cos\left(\omega t - \frac{x_i}{\delta_s} - \psi\right) \tag{2}$$

where x_i is the radial distance from the fluid–solid interface. From properties of Fourier transform, we can write, for a location x_i:

$$| Y_i | = A_0 e^{\frac{-x_i}{\delta_s}} \quad \text{and} \quad \text{angle}(Y_i) = \omega t - \frac{x_i}{\delta_s} - \psi \tag{3}$$

Temperature signals at locations x_i and x_j are obtained by measurement, Y_i and Y_j are their Fourier transforms. The experimental skin thickness δ_s can be computed by two methods at each location x_i. Either from the expression

$$\frac{| Y_j |}{| Y_i |} = e^{\frac{x_i - x_j}{\delta_s}} \tag{4}$$

which leads to δ_{s1} and δ_{s2} in Table 1, or from the expression

$$\text{angle}(Y_j) - \text{angle}(Y_i) = \frac{x_i - x_j}{\delta_s} \tag{5}$$

which leads to δ_{s3} and δ_{s4} in Table 1, where the theoretical skin thickness $\delta_{s,theo}$ computed by taking a heat diffusivity κ_s equal to $3.97 \times 10^{-6}\ m^2\ s^{-1}$ [19] for stainless steel. Considering the precision of measures for significant cases considered in Table 1, there is a relative good agreement with experimental and theoretical values of skin thicknesses.

3.2. Importance of temperature oscillations in the wall

In Fig. 4, we present the temperature evolution in the wall at 206.3 μm from the fluid–solid interface. We observe that the oscillation magnitude of temperature is about 0.1 K. The case considered here corresponds to a turbulent flow which is characterized by a dimensionless frequency and a Reynolds number among the highest of our experimental conditions [11]. This result confirms the usual hypothesis of neglecting temperature oscillations in the wall (see Section 1). Nevertheless, our instrumentation allowed us to detect them and to observe instantaneous local heat transfers at the solid–fluid interface.

Table 1
Comparison between analytical and experimental skin thicknesses

	Re_{max} = 97,605, Re_ω = 241.6	Re_{max} = 160,163, Re_ω = 144.15	Re_{max} = 205,445, Re_ω = 92.45
$\delta_{s,theo} = \sqrt{\frac{2\kappa_s}{\omega}}$ (mm)	0.69	0.90	1.10
δ_{s1} (mm)	0.65	0.78	0.85
δ_{s2} (mm)	0.78	1.00	1.10
δ_{s3} (mm)	0.73	0.67	0.95
δ_{s4} (mm)	0.77	0.81	1.10

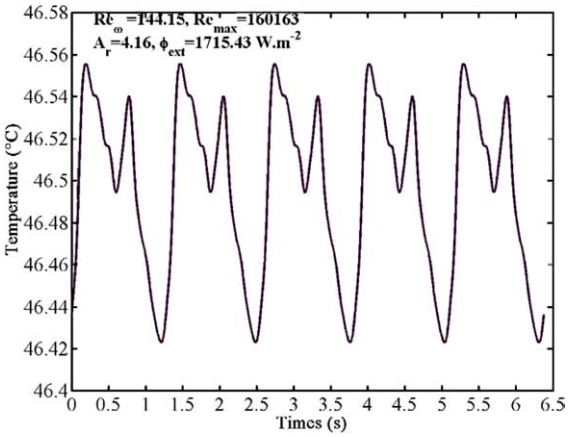

Fig. 4. Temperature evolution in the wall at 206.3 μm from the interface.

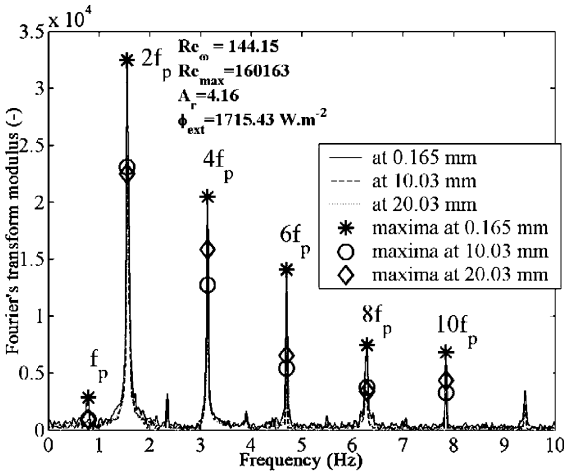

Fig. 6. Temperature signals in the fluid.

3.3. Influence of the wall on heat transfers

In Figs. 5 and 6, we represent Fourier's transforms of temperature measures at several radial positions, in the wall (Fig. 5) and in the fluid (Fig. 6), in the same experimental conditions as these in Fig. 4. We observe that predominant frequencies are not the same in the wall and in the fluid. Indeed, in the fluid, at the different radial locations observed, the most important frequency of the temperature evolution is twice the piston motion frequency (f_p). This "double frequency" reflects the two sweepings of fluid in one oscillation cycle [11]. In the wall, for the case considered, the piston motion frequency is predominant, whereas this frequency is barely detectable in fluid. From other experimental conditions studied [11], we observed that this phenomena is accentuated for cases characterized by the highest Re_{max} and Re_ω. The wall behaves like a low pass filter with respect to the thermal sollicitation imposed by the heated oscillating flow.

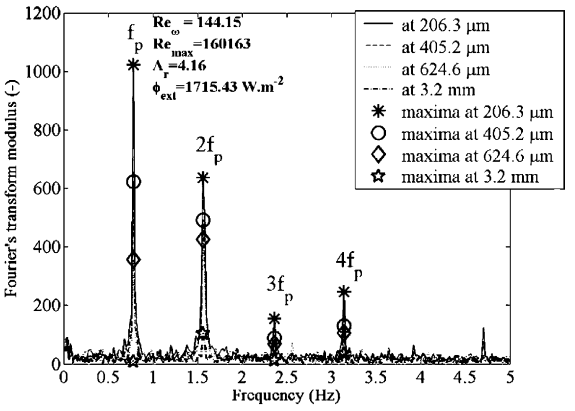

Fig. 5. Temperature signals in the wall.

4. Local heat transfer

4.1. Methodology

For some of our experimental conditions (high Re_{max} and Re_ω), we observe high temperature variations near the wall (Fig. 7). These cases are characterized by wall temperature and wall heat flux highly unsteady near the fluid–solid interface. For these cases, it is impossible to characterize local heat transfer by assuming constant wall temperature and wall heat flux. In order to precisely

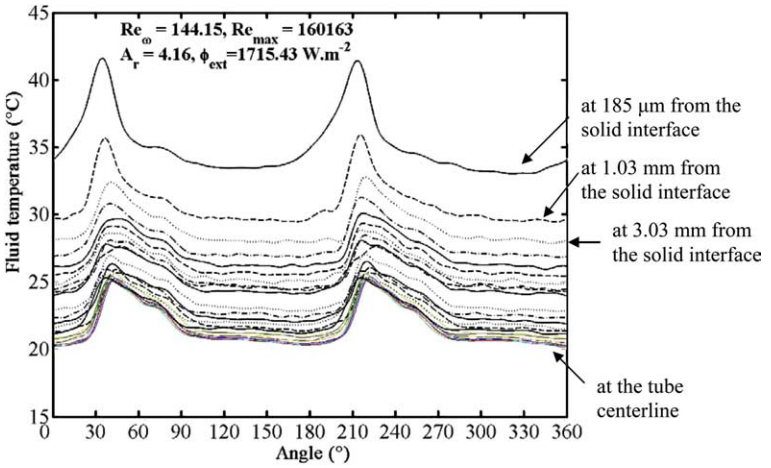

Fig. 7. All temperatures signals measured in the fluid.

determine local heat transfers, we apply inverse heat conduction principles on our measured temperatures. From measures of instantaneous temperature in the wall and from the analytical solution which gives the temperature evolution inside the wall, we determine the wall temperature and the wall heat flux at the fluid–solid interface as follows.

Knowing that $e_W \ll R_t$, the conduction equation in the wall can be written as follows:

$$\frac{\partial^2}{\partial x^2} T_s(x,t) = \frac{1}{\kappa_s} \frac{\partial}{\partial t} T_s(x,t) \tag{6}$$

The solution can be written as follows:

$$T_s(x,t) = T_{sp}(x) + T_{su}(x,t) \tag{7}$$

with

$$T_{sp}(x) = \left(\frac{\overline{T}_{s1} - \overline{T}_{s2}}{x_1 - x_2} \right)(x_1 - x_2) + \overline{T}_{s1} \tag{8}$$

and with $\alpha_k^2 = \frac{i2\pi f_k}{\kappa_s}$

$$T_{su}(x,t) = \sum_k (A_k e^{-\alpha_k x} + B_k e^{\alpha_k x}) e^{i2\pi f_k t} \tag{9}$$

From the Fourier's transforms Y_1 and Y_2 of the temperature signals measured at the locations x_1 and x_2 respectively, we can write:

$$A_k = Y_1 e^{\alpha_k x_1} - B_k e^{2x_1\alpha_k} \tag{10}$$

$$B_k = \frac{Y_2 - Y_1 e^{\alpha_k (x_1 - x_2)}}{e^{\alpha_k x_2} - e^{\alpha_k (2x_1 - x_2)}} \tag{11}$$

With this solution, we can determine the temperature at every location x in the wall.

In Fig. 8, in order to validate the methodology, we superpose the analytical solution in solid line with the measured signal in dashed line at the location $x_3 = 624.6$ μm. Considering the very low signal amplitude with respect to the noise level (0.075 °C) [11], the agreement between these curves is quite acceptable.

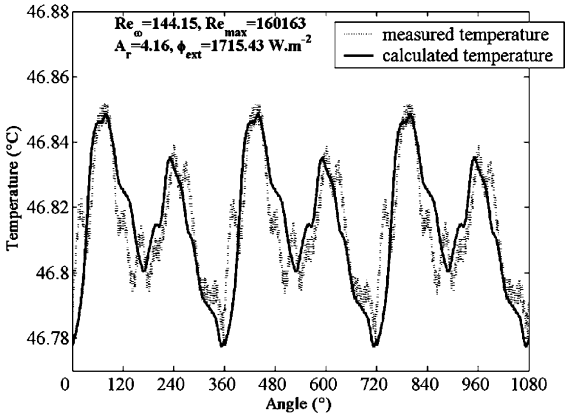

Fig. 8. Comparison between analytical solution and measured data in the wall at 624.6 μm from the interface.

4.2. Wall temperature at the fluid–solid interface

From the analytical solution (Eq. 8), we obtain the wall temperature at the solid–fluid interface ($x = 0$). In Fig. 9, we plot this analytical solution together with the three measured temperature signals in the wall.

Since thermocouples inserted in the wall are set up at very small distances from the wall ($x_1 = 206$ μm), uncertainties on extrapolated temperatures are quite close to the measure uncertainty at $x_1(u(T_1)) = 0.075$ °C). For example, for the case considered in Fig. 9, we have $Re_\omega = 144.15$ which leads to a theoretical skin thickness $\delta_s = 0.90$ mm (Table 1). The uncertainty on the amplitude of the surface temperature oscillations is thus:

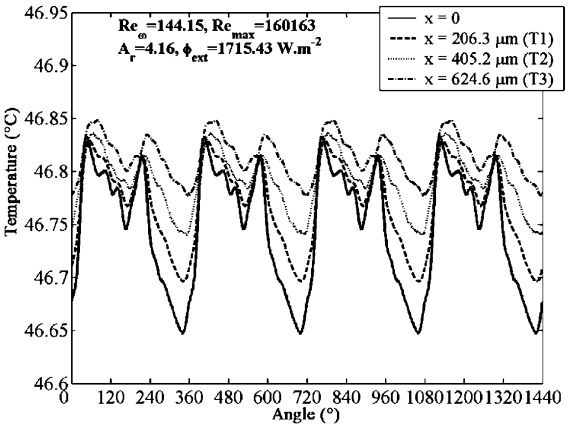

Fig. 9. Temperature signals in the wall and at the interface (solid line).

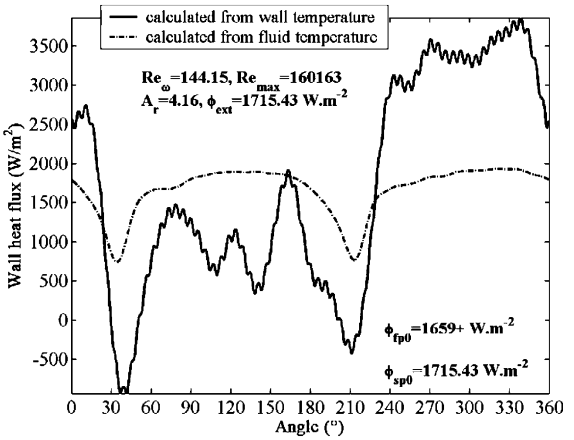

Fig. 10. Evolutions of the wall heat flux calculated by two methods.

$$u(T_0) \cong e^{\frac{x_1}{\delta_s}} u(T_1) \cong 1.26u(T_1) \tag{12}$$

We have thus $u(T_0) < 0.1$ °C. With this result, we can see the interest and originality of the parietal sensor.

4.3. Wall heat flux density

4.3.1. First method: determination from measures in the wall

The unsteady component of the wall heat flux density is obtained by derivation of the analytical solution of temperature $T_{su}(x,t)$, such as:

$$\phi_s(x,t) = \phi_{sp} - k_s \sum_k (-\alpha_k A_k e^{-\alpha_k x} + \alpha_k B_k e^{\alpha_k x}) e^{i2\pi f_k t} \tag{13}$$

where ϕ_{sp} is the permanent component of the wall heat flux imposed at the external surface by the heater band. The value of this expression in $x = 0$, ϕ_{s0}, gives the wall heat flux density at the fluid–solid interface, obtained from temperature measures in the wall.

4.3.2. Second method: determination from the measures in the fluid

The wall heat flux is computed from the wall temperature at $x = 0$, T_{s0}, and the fluid temperature at the radial location $\Delta r = 0.185 \times 10^{-3}$ m from the interface, T_{f1}. From these temperatures, heat flux density can be approached by the linearized expression:

$$\phi_{f0} = k_f \frac{(T_{s0} - T_{f1})}{\Delta r} = \phi_{fp0} + \phi_{fu0} \tag{14}$$

For the case characterized in Fig. 10, the evolution of the wall heat flux given by the first method is drawn in solid line whereas the dashed line corresponds to the wall heat flux obtained from the measure of fluid temperature taken at 185 ± 3 μm from the interface. This comparison allowed us to test the validity of the determination method which uses measures of fluid temperature exclusively, as used by some authors [10].

Theoretically, the permanent composant (ϕ_{fp0}) of wall heat flux obtained from fluid temperature and the approximate equation (Eq. (14)) should have a value slightly lower than the one of the permanent composant of wall heat flux (ϕ_{sp0}) obtained from the more accurate inverse method and wall temperatures. (In fact, at the fluid–solid interface, these values should be strictly equal but the approximate value of fluid temperature derivative in the boundary layer is lower than the true one at the fluid–solid interface). Regarding the permanent components of the wall heat flux (ϕ_{fp0} and ϕ_{sp0}) in Fig. 10, this is effectively the case here.

Concerning the unsteady evolutions, they are not in agreement. The distance from the wall (0.185 mm) is probably too high. The fluid is not at rest in this area and there is a convective exchange of heat added to the conductive exchange. In our case, the second method does not allow the estimation of unsteady variations of the wall heat flux at the interface. So, the first method gives a value of heat flux density closer to the true value.

Concerning wall heat flux computed from the first method (from wall temperature), we observe negative values for some angles, such as around 30° and 210°. It means that, at these local times, there is inversion of the wall heat flux direction: The direction of heat transfer is reversed twice in an oscillation cycle.

5. Dimensionless heat flux

The usual way to characterize heat transfer phenomena is to refer to the Nusselt number defined as follows:

$$Nu = \frac{\phi D_t}{k_f(T_w - T_b)} \tag{15}$$

where T_b is the bulk temperature such as

$$T_b = \frac{\int_0^{R_t} u(x,r,t)T_f(x,r,t)r\,dr}{\int_0^{R_t} u(x,r,t)r\,dr} \tag{16}$$

where $u(r,x,t)$ is the instantaneous fluid velocity in the tube. Two problems arise when trying to describe oscillating flow heat transfer with this traditional approach.

The first problem comes up from the use of the bulk temperature in the definition. Indeed, in the case of oscillating flow the bulk temperature takes infinite values twice a cycle [11]. To avoid this problem, we replace this bulk temperature by the instantaneous temperature averaged over the tube section T_m, such as:

$$T_m = \frac{2}{R_t^2}\int_0^{R_t} rT(r,t)\,dr \tag{17}$$

In order to characterize local heat transfer, this cross-averaged temperature should be adequate [11].

The second problem deals with terminology. As the heat transfer can suffer direction changes during the cycle, the usual denomination of Nusselt number may be not appropriate. It seems more suitable to define a dimensionless heat flux instead of a classical Nusselt number.

So, defining an arbitrary reference heat flux density by

$$\phi_{ref} = \frac{k_f}{D_t}(T_w - T_m) \tag{18}$$

we introduce the dimensionless heat flux density ϕ^* by the following relationship:

$$\phi^* = \frac{\phi}{\phi_{ref}} = \frac{\phi D_t}{k_f(T_w - T_m)} \tag{19}$$

The dimensionless heat flux density ϕ^* has the same mathematical form as the usual Nusselt number.

We can now compare dimensionless heat flux densities obtained either from local temperature and wall heat flux at the fluid–solid interface or from external wall temperature and wall heat flux supplied by the heater band at the external wall.

5.1. Local dimensionless heat transfer

From the wall heat flux and the wall temperature at the fluid–solid interface, taking ($T_w = T_{s0}$), we can define the local dimensionless heat flux density ϕ^*_{s0} as follows:

$$\phi^*_{s0} = \frac{\phi_{s0} D_t}{k_f(T_{s0} - T_m)} = \frac{\phi_{s0}}{\phi_{ref}} \tag{20}$$

In order to avoid negative values of this dimensionless heat flux twice in an oscillation cycle, we used a complex formulation [20,21]. This formulation is meaningful since it gives not only the magnitude of the heat transfer but also an information about the phase shift between the wall heat flux ϕ_{s0} and the temperature difference $(T_{s0} - T_m)$.

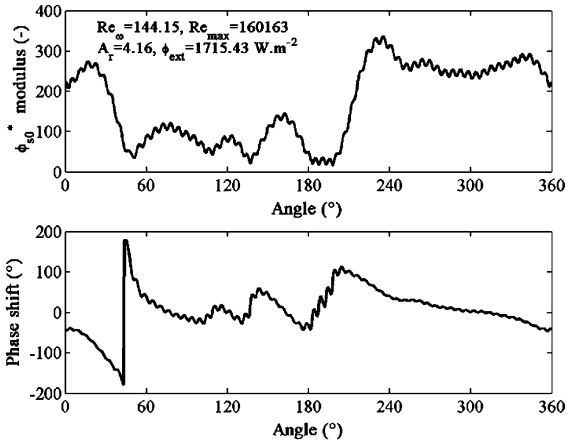

Fig. 11. Evolution of the local dimensions heat flux density.

For the case considered in Fig. 11, we observe the absence of symmetry between both halves of the oscillation cycle. This observation is tied up with that of Section 3.3: frequency corresponding to the piston movement is predominant in the wall and this phenomenon influences heat transfer at the interface. By comparison between Figs. 10 and 11, we can see that evolutions of the dimensionless heat flux and wall heat flux have the same predominant frequencies.

5.2. Overall dimensionless heat transfer

Considering heat exchange between the external surface of the tube where heat is generated by the band heater and the fluid inside the tube, taking wall heat flux (ϕ_{ext}) and temperature ($T_{s,ext} = T_w$) constant on the external wall, the expression of the overall dimensionless heat flux density ϕ^*_{ext} becomes:

$$\phi^*_{ext} = \frac{\phi_{ext} D_t}{k_f(T_{s,ext} - T_m)} = \frac{\phi_{ext}}{\phi_{ref}} \tag{21}$$

By using the complex formulation, we obtained the curves shown in Fig. 12. In this case, the evolution of the overall dimensionless heat flux density is directly related to the cross-averaged temperature T_m since ϕ_{ext} and $T_{s,ext}$ are constant. This formulation leads to a symmetrical evolution since we use fluid temperature measures.

Local and overall dimensionless heat flux density ϕ^*_{s0} and ϕ^*_{ext} have very different evolutions. Their maxima are not at the same moments in the oscillation cycle and the amplitude variations of the local dimensionless

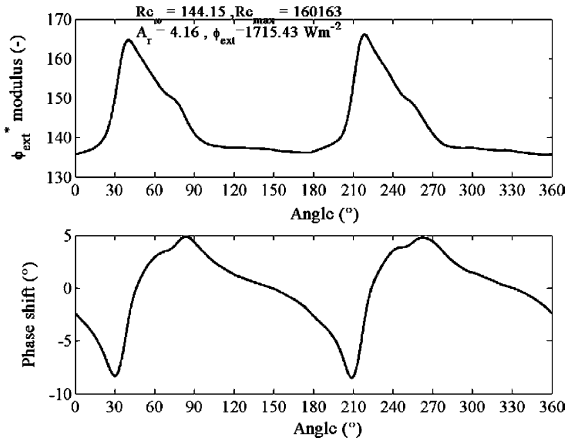

Fig. 12. Evolution of the global dimensionless heat flux density.

heat flux are more important than those of the overall dimensionless heat flux.

It is clear that these dimensionless heat flux definitions appear to be inadequate in oscillating flow and a deepest analysis is needed to propose a more appropriate formulation allowing to better characterize instantaneous heat transfer in this type of flow.

Other studies dealing with heat transfer in oscillating flow do not have the same objectives as ours. Some of them determine a space–time averaged Nusselt number [9] in another domain of dimensionless frequency and tidal displacement or impose a constant temperature at the exterior wall [8]. Other studies impose another temporal signal to the pressure [2] or determine a length-averaged and a cycle-averaged local Nusselt number in porous media [22]. In these conditions, we cannot compare our results with those from other works because presently available published results do not give details on instantaneous local heat transfer or use other boundary conditions.

6. Conclusion

We built an instrumented test rig which allowed us to study heat transfer in oscillating flow. The generated flow is purely oscillatory because we observe a good agreement between velocity profiles measured by laser Doppler anemometry and theoretical ones, in laminar flow.

Magnitudes of signals measured inside the wall, near the fluid–solid interface, are small but reliable. In fact, we find a good agreement between experimental and theoretical skin thicknesses. Temperature measurements allow us to verify that the hypothesis of neglecting temperature oscillations in the wall is acceptable since we detect variations of 0.1 K in cases characterized by the highest $Re_{\max}$ and Re_{ω} in our experimental conditions. Nevertheless, we are able to use them to observe the wall effect on heat transfers and to characterize local heat transfer at the interface by using heat conduction inverse methods. We show that fundamental frequencies are not the same in the wall and in the fluid, as if the wall acts like a low pass filter on the fluid temperature signal.

The determination of the heat flux by using wall temperatures exclusively or fluid temperatures measured near the interface leads to different results. The location of the thermocouple in the fluid is too far from the interface and we cannot consider the fluid at rest at 185 μm from the interface, in the conditions of flow considered here.

Differences found between the overall and local dimensionless heat flux density raise the question of the usefulness of a quantity which would, in oscillating flow conditions, play the same role as the Nusselt number in more usual conditions.

References

[1] R. Smith, Contaminant dispersion in oscillatory flow, J. Fluid Mech. 114 (1982) 379–398.
[2] L.A.O. Rocha, A. Bejan, Geometric optimization of periodic flow and heat transfer in a volume cooled by parallel tubes, J. Heat Transfer 123 (April) (2001) 233–239.
[3] D.M. Eckmann, J.B. Grotberg, Experiments on transition to turbulence in oscillatory pipe flow, J. Fluid Mech. 222 (1991) 329–350.
[4] A.J. Organ, Thermodynamics and Gas Dynamics of the Stirling Machines, Cambridge University Press, 1992.
[5] T.W. Simon, J.R. Seume, A survey of oscillating flow in Stirling engine heat exchangers, NASA Contractor Report 182108, 1988.
[6] R.C. Tew, S.M. Geng, Overview of NASA supported Stirling thermodynamics loss research, IECEC 92, Paper 929462, 1992, pp. 5489–5494.
[7] D. Gedeon, GLIMPS Version 3.0 User's manual. Gedeon Associates, South Canaan road, Athens, OH 45701, 1990.
[8] T. Zhao, P. Cheng, A numerical solution of laminar forced convection in a heated pipe subjected to a reciprocating flow, Int. J. Heat Mass Transfer 38 (16) (1995) 3011–3022.
[9] T. Zhao, P. Cheng, Oscillatory heat transfer in a pipe subjected to a laminar reciprocating, J. Heat Transfer 118 (3) (1996) 592–597.
[10] S. Qiu, T.W. Simon, Measurements of heat transfer and fluid mechanics within an oscillatory flow in a pipe, Fund. Heat Transfer Forced Convection, ASME-HTD (285) (1994) 1–8.
[11] P. Bouvier, Transferts thermiques en écoulement oscillant: Application au moteur Stirling, Ph.D. Thesis, Université de Nantes, Nantes, France, 2000.
[12] B.F. Blackwell, R.J. Moffat, Design and construction of a low-velocity boundary layer temperature probe, J. Heat Transfer (1975) 313–315.
[13] B. Bourouga, V. Goizet, J.-P. Bardon, Les aspects théoriques régissant l'instrumentation d'un capteur thermique

pariétal à faible inertie, Int. J. Thermal Sci. 39 (1) (2000) 96–109.
[14] H.B. Atabek, C.C. Ghang, Oscillatory flow near the entry of circular tube, ZAMP 12 (1961) 403–422.
[15] S. Uchida, The pulsating viscous flow superposed on the steady laminar motion of incompressible fluid in a circular pipe, Z. Angew. Math. Phys. 7 (1956) 403–422.
[16] E.J. Watson, Diffusion in oscillatory pipe flow, J. Fluid Mech. 133 (1955) 233–244.
[17] P. Bouvier, P. Stouffs, J.-P. Bardon, Transition laminaire-turbulent en écoulement oscillant en conduite cylindrique: approche expérimentale par anémométrie laser et mesures thermiques, Actes du Congrés SFT 2001, Elsevier, Paris, 2001, pp. 57–62.
[18] J.R. Seume, G. Friedman, T.W. Simon, Fluid mechanics experiments in oscillatory flow, Vol. 1: Report NASA Contractor Report 189127, Vol. 2: Tabulated Data NASA Contractor Report 189128, March 1992.
[19] J.F. Sacadura, Initiation Aux Transferts Thermiques, Lavoisier TEC & DOC, France, 1980.
[20] D. Gedeon, 1986, Mean-parameter modeling of oscillating flow, J. Heat Transfer 108 (1986) 513–518.
[21] A.A. Kornhauser, J.L. Smith Jr., Heat transfer with oscillating pressure and oscillating flow, 24th IECEC 5 (1989) 2347–2353.
[22] K.C. Leong, L.W. Jin, An experimental study of heat transfer in oscillating flow through a channel filled with an aluminium foam, Int. J. Heat Mass Transfer 48 (2005) 243–253.